

Wild emmer introgression alters root-to-shoot growth dynamics in durum wheat in response to water stress

Harel Bacher ^{1,2}, Feiyu Zhu,³ Tian Gao,³ Kan Liu,⁴ Balpreet K. Dhatt,² Tala Awada ⁵, Chi Zhang,⁴ Assaf Distelfeld,⁶ Hongfeng Yu ³, Zvi Peleg ¹ and Harkamal Walia ^{2,*†}

- 1 The Robert H. Smith Institute of Plant Sciences and Genetics in Agriculture, The Hebrew University of Jerusalem, Rehovot, Israel
- 2 Department of Agronomy and Horticulture, University of Nebraska-Lincoln, Lincoln, Nebraska, USA
- 3 Department of Computer Science and Engineering, University of Nebraska-Lincoln, Lincoln, Nebraska, USA
- 4 School of Biological Sciences, University of Nebraska-Lincoln, Lincoln, Nebraska, USA
- 5 School of Natural Resources, University of Nebraska-Lincoln, Lincoln, Nebraska, USA
- 6 The Institute of Evolution, University of Haifa, Haifa, Israel

*Author for communication: hwalia2@unl.edu

†Senior author.

H.B., H.W., T.A., and Z.P. designed the experiments. Z.P. and A.D. generated genetic materials. H.B. and B.D. conducted physiological and transcriptome experiments. F.Z., T.G., and H.Y. processed the image data. H.B., K.L., and C.Z. performed transcriptome data analysis. H.B., H.W., and Z.P. wrote the paper. All authors have read and approved the manuscript.

The author responsible for distribution of materials integral to the findings presented in this article in accordance with the policy described in the Instructions for Authors (<https://academic.oup.com/plphys/pages/general-instructions>) is: Harkamal Walia (hwalia2@unl.edu).

Abstract

Water deficit during the early vegetative growth stages of wheat (*Triticum*) can limit shoot growth and ultimately impact grain productivity. Introducing diversity in wheat cultivars to enhance the range of phenotypic responses to water limitations during vegetative growth can provide potential avenues for mitigating subsequent yield losses. We tested this hypothesis in an elite durum wheat background by introducing a series of introgressions from a wild emmer (*Triticum turgidum* ssp. *dicoccoides*) wheat. Wild emmer populations harbor rich phenotypic diversity for drought-adaptive traits. To determine the effect of these introgressions on vegetative growth under water-limited conditions, we used image-based phenotyping to catalog divergent growth responses to water stress ranging from high plasticity to high stability. One of the introgression lines exhibited a significant shift in root-to-shoot ratio in response to water stress. We characterized this shift by combining genetic analysis and root transcriptome profiling to identify candidate genes (including a root-specific kinase) that may be linked to the root-to-shoot carbon reallocation under water stress. Our results highlight the potential of introducing functional diversity into elite durum wheat for enhancing the range of water stress adaptation.

Introduction

Water deficit is the major limiting factor during early season wheat (*Triticum*) vegetative growth, causing subsequent yield losses (Passioura and Angus, 2010). Water limitation

during early season vegetative stage causes yield losses due to the reduced supply of assimilates to grains. Moreover, in recent years, climate change has led to increased fluctuation of precipitation. Durum wheat (*Triticum turgidum* ssp.

durum (Desf.) MacKey; $2n = 4x = 28$, genome BBAA) is mainly grown in the semi-arid Mediterranean Basin and also across North and East Africa, Europe, North America, India, and Australia (Fuerst-Bjeliš, 2017; Royo et al., 2017). In the Mediterranean Basin, durum wheat is mainly cultivated under rain-fed conditions and yields are thus highly affected by year-to-year and within-year precipitation fluctuations (Peleg et al., 2008). One approach for improving the performance under drought conditions is to select durum cultivars with morpho-physiological adaptive mechanisms, such as early vigor, enhanced water-use efficiency (WUE), and yield stability under water-limiting environments (Araus et al., 2002). The use of landraces and wild relatives of wheat that are adapted to dry environments can be a potential genetic resource for these traits (Reynolds et al., 2017).

The ability to maintain higher biomass under water-limiting conditions is directly linked to photosynthetic capacity, which can translate into higher yield in many crops and environments (Zelitch, 1982; Ashley and Boerma, 1989). Phenotypic characterization of early vegetative growth traits under field conditions is challenging due to high spatial variability in the soil moisture profile across a field and unpredictable incidence of multiple biotic and abiotic factors (Pauli et al., 2016; Furbank and Tester, 2011). Since vegetative shoot growth in wheat can be considered an important trait to measure on a temporal scale, it can be challenging to discern the consequence of introducing new alleles or genes from wild relatives into cultivated lines when assessing early vegetative growth stages in field studies. Capturing the phenotypic variation in shoot growth for genetic analysis requires accurate, temporal measurements under controlled conditions that limit the influence of environmental factors not included as experimental variables. With technological advancements in close range, nondestructive imaging platforms, recording the temporal shoot growth dynamics of individual plants under water stress in controlled growth conditions is more tractable (Jin et al., 2021).

Root responses to water stress are less studied than shoot responses due to inherently higher root plasticity and difficulty in accurately measuring their phenotypic traits (Uga, 2021). Wheat breeding has reduced the root biomass in modern varieties relative to their wild progenitors (Waines and Ehdai, 2007; Golan et al., 2018; Fradgley et al., 2020), a trend which accelerated during the “Green Revolution” (Langridge and Reynolds, 2021). A higher photosynthetic cost of root growth and respiration led to allelic enrichment favoring reduced carbon allocation to roots when selections were made under optimal environments (Lambers et al., 2002). Under water-stress conditions, shoot growth is restricted as more carbon is allocated to roots, which results in a higher root-to-shoot ratio (Correa et al., 2019). Deeper roots and more lateral root growth enable the plant to access more water during grain filling (Campos et al., 2004). The resulting greater stomatal conductance, cooler canopies, and maintenance of physiological activity can mitigate yield losses (Kirkegaard et al., 2007). Optimal root-to-shoot

partitioning produces a balance between productivity and root water absorption (Voss-Fels et al., 2018) and plays a key role in drought adaptation. Although the phenotypic range of elite durum germplasm for root morphology has been examined, changes in root–shoot resource allocation under water limitation is not well-explored (Kara et al., 2000; Sayar et al., 2007). One way to enhance root-to-shoot phenotypic plasticity is by introducing wild alleles in elite durum backgrounds to increase adaptation to water stress. Phenotypic plasticity in this context is defined as the range of phenotypic divergence in response to an environmental stimulus. Phenotypic plasticity is a genetic trait and has the potential to increase the range of adaptation of a species with increase in genetic variation (Bradshaw, 2006; Jump et al., 2009; Chevin et al., 2010).

Wild emmer wheat [*T. turgidum* ssp. *dicoccoides* (Körn.) Thell], the direct allotetraploid ($2n = 4x = 28$; genome BBAA) progenitor of domesticated wheat, thrives across the Fertile Crescent in a wide eco-geographic range. Wild emmer exhibits robust vegetative growth under arid conditions and can serve as a potential source for enhancing drought adaptation in durum wheat (Peleg et al., 2005; Avni et al., 2014). The potential for wild emmer to change wheat adaptation to water stress was recently demonstrated for root traits (Golan et al., 2018; Hendel et al., 2021). In this study, we have used a set of wild emmer introgression lines (ILs) in an elite durum wheat background to discover divergent phenotypic responses to water stress, using a high temporal resolution imaging platform. We tested the hypothesis that wild introgression can expand the range of phenotypic responses to water stress in domesticated wheat due to increased genetic variation. We identified two contrasting water stress response strategies, ranging from phenotypic stability to plasticity, and characterized representative ILs for these two strategies to gain further physiological insights. One of the ILs exhibiting a change in root-to-shoot ratio in response to water stress was used for genetic and transcriptomic analysis to identify candidate genes (CGs) localizing to the wild emmer introgressions. Our study highlights the potential of increasing genetic variation through wild introgressions to promote various water stress-responsive dynamics, as well as characterization of water stress adaptive mechanisms that can enhance wheat adaptation to water stress.

Results

Wild emmer introgressions confer divergent water stress responses

The goal of this study was to investigate if the introduction of wild emmer introgressions can expand the range of phenotypic responses to water stress in an elite wheat cultivar background. To accomplish this, we used a set of wild emmer ILs (Oren, 2020). Zavitan was the wild donor parent, which was selected based on its high productivity and WUE under water stress (Supplemental Figure. S1). We used an image-based phenotyping approach to characterize a set of ILs tested during the early growth (i.e. vegetative) phase

under well-watered [WW; 80% field capacity (FC)] and water-limited (WL; 30% FC) conditions. Overall, the growth curves based on projected shoot area (PSA; as an estimator of shoot biomass; Supplemental Figure S2) of Svevo (the elite durum wheat cultivar) were similar to the median response of all ILs collectively during the experiment, thus supporting this experimental rationale (Supplemental Figure S3A). Other morphological traits such as plant width and architecture (convex area) also exhibited similar patterns (Supplemental Figure S3, C and D). The temporal imaging for shoot growth was combined with daily estimation of water loss from each pot, enabling us to determine soil moisture status during the experiment. Although most of the ILs reached the target of 30% FC in the WL treatment after an average of 19 d after transplanting (DAT), ranging from 14 to 24 DAT, many exhibited a reduction in biomass accumulation as early as 10 DAT (collectively), indicating an early water stress response as well as divergence in shoot growth response among the ILs (Supplemental Figure S4).

To examine the consequences of early water-stress response, we plotted the density distribution of the ILs under WW and WL treatments from the shoot imaging dataset. The ILs exhibited a broad range for all traits with Svevo positioned close to the average value for most traits (Figure 1A). Overall, the ILs showed a strong reduction in PSA as evident from the separation of the distribution curves in response to water stress. Under WL treatment, the phenotypic distribution of PSA was less dispersed compared with the WW treatment. A relatively smaller separation between treatments was observed for plant width and WUE. Notably, the phenotypic range of WUE varied more under WL compared to the WW treatment. Svevo's stress susceptibility index (S) for PSA (S-PSA), density (S-density), and WUE (S-WUE) indicated relatively stable morphological and physiological responses to the water stress (Supplemental Figure S5). Higher responsiveness to water stress would be indicated by high values of S-WUE and smaller values of S-PSA (Peleg et al., 2005).

Understanding the relationship between morpho-physiological traits can provide better insights into key determinants of the expanded phenotypic range among the ILs. Correlation analysis between these traits at the 35 DAT time point showed a positive correlation between PSA and all morphological traits. Under WL treatment, PSA and plant density were positively correlated with WUE, suggesting that plant architecture can affect the WUE under stress (Figure 1B; Supplemental Table S1). Hierarchical clustering analysis of the morpho-physiological traits under WL treatment, and relative stress index traits, enabled us to classify the ILs into five groups that we broadly describe as Cluster 1 [high productivity and high stability (HPHS); consists of 6 ILs], Cluster 2 [high productivity and high plasticity (HPHP); consists of 10 ILs], Cluster 3 [moderate productivity and high plasticity (MPHP); consists of 13 ILs], Cluster 4 [low productivity and moderate plasticity (LPMP); consists of 11 ILs and Svevo], and Cluster 5 [low productivity and high stability (LPHS); consists of 7 ILs; Figure 2A]. In this context, we define

productivity as biomass accumulation under WL and plasticity as the genotype's ability to alter its phenotypic traits in response to water stress. Svevo resolved to Cluster 4 (LPMP), which is characterized by an intermediate response to water stress. The two most productive clusters (HP) showed differential stress response as expressed in the drought susceptibility index. Clusters HPHS and HPHP had the highest WUE under WL treatment with contrasting S-PSA. Cluster HPHS presented low values indicating high stability of biomass gain under WL compared to WW. Cluster HPHP's high S-PSA values indicated high plasticity for water stress in these ILs. Also, the discernable morphological characteristics were consistent with the clustering analysis (Figure 2B). The bootstrapping scheme shows that Clusters 2 and 5 have mean Jaccard similarities of 0.75 and 0.76, respectively, which indicates that clustering is stable (Figure 2A); Clusters 1, 3, 4 had means of 0.68, 0.64, 0.60, respectively, which indicates patterns in the clustering but consists of specific points that could belong to different clusters (Hennig, 2008). In addition, we conducted a silhouette clustering method for cluster consistency. The silhouette value is a measure of how similar an object is to its own cluster compared to other clusters. The silhouette ranges from -1 to $+1$, where a high value indicates that the object is well matched to its own cluster and poorly matched to neighboring clusters. The average silhouette score of 0.57 indicates a good cluster fitting (Figure 2C).

To uncover the relationships between traits and IL clusters, we conducted a principal component analysis (PCA) of the traits under WL treatment and in terms of drought susceptibility index (S). PCA identified three major PCs (eigenvalues > 1.2) accounting collectively for 76% of the phenotypic variance among the ILs (Figure 2B; Supplemental Figure S6). PC1 explained 36.9% of total variation and related positively with PSA, plant height, plant architecture, WUE, and plant density. PC2 explained 25.7% of the total variation and related positively with plant width, S-PSA, and S-density and negatively with S-WUE. PC3 explained 13.4% of the total variation and was positively related to WUE, S-PSA, and plant density (Supplemental Figure S6B). From the S-index perspective, high S-PSA, which reflects significant biomass reduction due to water stress, is associated with low S-WUE and confirmed that without WUE adaptation, plants will reduce their biomass gain under water stress. The IL visible morpho-physiological characteristics corresponded with the clustering analysis (Figure 2C).

Water stress-responsiveness classification is based on temporal growth dynamics

To better understand the temporal dynamics of shoot growth, we mapped the overall trajectories and phenotypic distributions of these traits on a weekly basis (Figure 3A). In general, all clusters exhibited higher biomass accumulation and higher coefficient of variance (CV) under WW

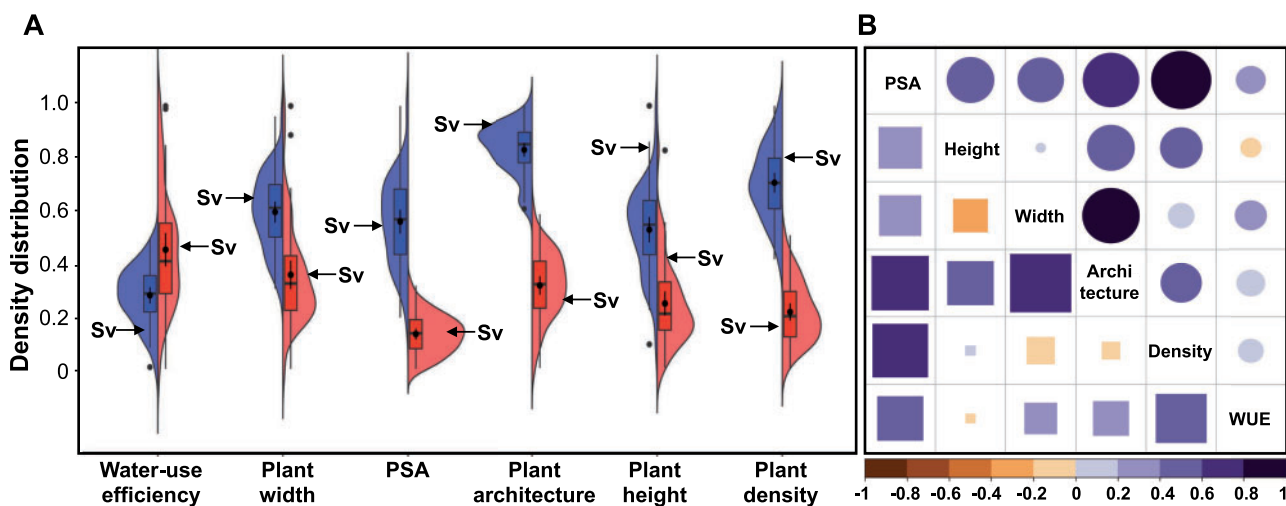


Figure 1 Wild emmer introgressions promote phenotypic diversity in elite durum cultivar. **A**, Density distribution of morpho-physiological traits for 47 ILs under WW (blue) and WL (red) treatments. WUE, plant width, PSA, plant architecture (Convex area), plant height, and plant density. The vertical lines below and above each box plot represent the 10th and 90th percentiles, respectively. The box plot bottom and top limits represent the 25th and 75th percentile and the line inside the box represents the median (50 percentile). $n = 48$. The parental line Svevo (Sv) is marked with an arrow. **B**, Pearson correlation matrix between morpho-physiological traits under WW and WL treatments. Circles represent correlations within the WW treatment and squares within the WL treatment. Colors and size indicate the level of correlation (r) from positive correlation (purple) to negative (brown). $n = 48$.

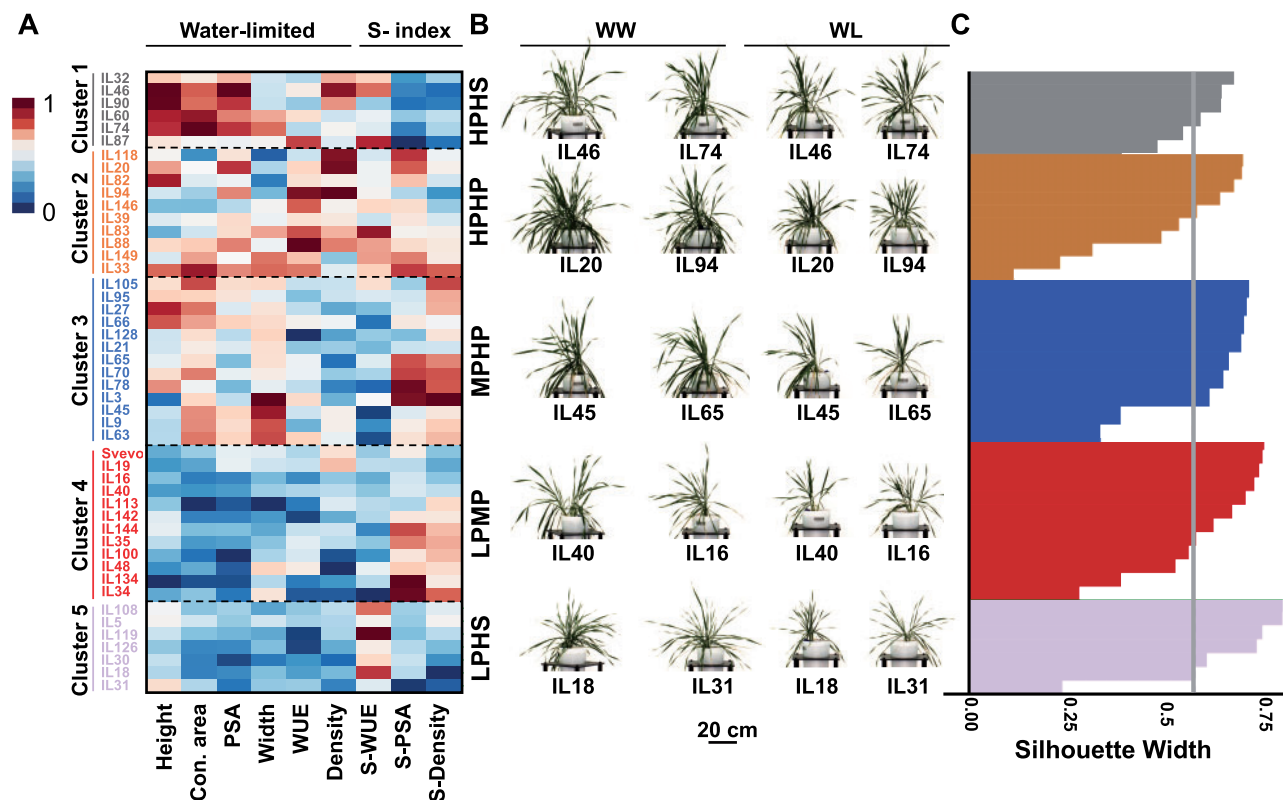


Figure 2 Shoot phenotypic response-based clustering of ILs and elite parent. **A**, Hierarchical clustering integrated heat map of morpho-physiological traits under WL treatment and as expressed in drought susceptibility index (S) on the last day of the experiment ($n = 3$). PSA, plant height (Height), plant width (Width), plant architecture (Con. area), plant density (Density), WUE. Clustering analysis separated the ILs into five distinct clusters according to the Ward method; clusters were named by the cluster characteristics. The heat map colors from blue to red represent lower to higher scaled values, respectively. We broadly describe the clusters as follows: Cluster 1 (HPHS; gray), Cluster 2 (HPHP; orange), Cluster 3 (MPHP; blue), Cluster 4 (LPMP; red), and Cluster 5 (LPHS; purple). **B**, Representative images of ILs from each responsiveness cluster under WW and WL treatments at 35 days after transplanting. **C**, Silhouette width to evaluate the clustering consistency, where the gray line represents the Silhouette score.

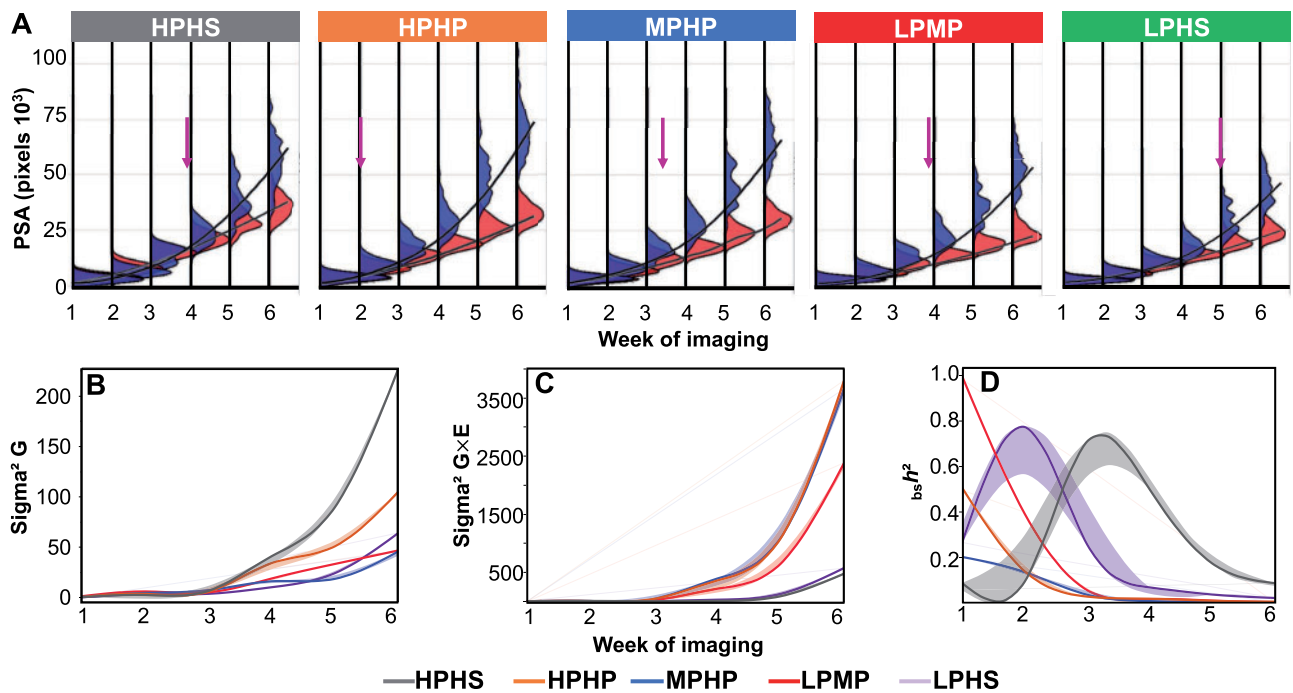


Figure 3 Time series dynamics of the five responsiveness clusters. A, Temporal frequency distribution of biomass accumulation (PSA) of each water stress-responsive cluster under WW (blue) and WL (red) treatments. The five clusters are: HPHS (gray), HPHP (orange), (MPHP; blue), LPMP (red), LPHS (purple). The time point of significant difference in response to water stress is marked with an arrow (t test, $P \leq 0.05$; $n = 6$ for HPHS, $n = 10$ for HPHP, $n = 13$ for MPHP, $n = 12$ for LPMP, $n = 7$ for LPHS). Temporal heritability components of (B) genetic ($\sigma^2 G$), (C) environmental interaction ($\sigma^2 G \times E$), and (D) broad-sense heritability ($bs h^2$). Continuous lines represent the smooth curve through the data and the shaded area represents the standard error of the smooth curve ($n = 6$ for HPHS, $n = 10$ for HPHP, $n = 13$ for MPHP, $n = 12$ for LPMP, $n = 7$ for LPHS).

relative to WL treatment (Figure 3A; Supplemental Table S2). The PSA distributions under WW and WL treatments showed that the high stability (HS) clusters exhibited substantial overlap between the WW and WL curves in weeks 5 and 6. The point of significant response to water stress was determined when three contiguous days of significant ($P < 0.05$) difference in growth between treatments was recorded, which ranged from 10 DAT (HPHP cluster) to 26 DAT (HPHS cluster; Figure 3A; Supplemental Table S3). A similar pattern was found for plant architecture and density (Supplemental Figure S7). The parental line (Svevo; LPMP cluster) expressed an intermediate response (17, 18, and 15 DAT for PSA, plant architecture, and density, respectively; Supplemental Figure S7). Although the MPHP cluster exhibited high biomass accumulation under WW treatment, it was labeled as moderate productivity (MP) based on its performance under WL treatment. Cluster classification to productivity (i.e. HP, MP, and LP) was found to be significantly different ($P < 10^{-4}$, LSMean Differences) under WL. This analysis enabled us to capture the temporal dynamics, which are typically challenging to determine without extensive destructive sampling.

Plant responsiveness clusters expressed in heritability dynamics

To dissect the genetic (G) and environmental (E) components of PSA underlying each responsiveness cluster through

developmental stages, we calculated broad-sense heritability and its components. The HPHS cluster exhibited the largest genetic component ($\sigma^2 G$), which increased with the progression of water stress duration (Figure 3B). On the other hand, HPHP and MPHP clusters had smaller genetic components and the highest $G \times E$ interaction ($\sigma^2 G \times E$; Figure 3, B and C). The broad-sense heritability dynamics ($bs h^2$) of PSA showed clear separation into stability (LPHS and HPHS) and plasticity (LPMP, MPHP, and HPHP; Figure 3D). In general, the level of PSA $bs h^2$ decreased over time. Heritability dynamics of plant density showed a strong genetic component for HPHP and a large environmental effect for LPMP that increased over time. Plant architecture presented a large environmental effect on MPHP, causing low $bs h^2$ for this cluster (Supplemental Figure S8). Overall, the heritability dynamics of the responsiveness clusters emphasized that stability and plasticity derived from both genetic and environmental effects within the IL panel.

IL20 exhibited a higher assimilation rate under WL conditions

We next focused on the phenotypic plasticity/stability under WL by comparing two high productivity clusters, HPHP and HPHS, represented by IL20 and IL46, respectively, for downstream physiological analysis. We targeted the temporal window during early growth stages (15–19 Zadoks scale; Zadoks et al., 1974), and used the same experimental

design that previously enabled us to categorize ILs based on the growth rate and water stress response. Under WL treatment, the relative growth rate dynamics demonstrated the advantage of the two productive clusters as expressed in higher linear equation slopes, 452.3 for IL20 and 558.1 for IL46, compared to Svevo (284.45; $P < 0.005$; Figure 4A; Supplemental Table S4). Under WW treatment, only IL20 had a higher slope compared to Svevo ($P = 0.001$). While IL46 maintained a similar linear equation slope under both water treatments (representing the high stability cluster), IL20 exhibited a significant change in the regression pattern, from 849.75 under WW to 452.32 under WL ($P < 10^{-3}$; Figure 4A), consistent with its selection based on high plasticity.

To complement the imaging, we also measured gas exchange parameters during the experiment. The average assimilation rate (A) declined with the progression of water stress as expected, with Svevo exhibiting the most reduction (37.7%), whereas the high stability IL46 had only 22.9% reduction (Figure 4B). Notably, IL20 exhibited the highest assimilation rate under WW treatment over time ($30.19 \mu\text{mol m}^{-2} \text{s}^{-1}$), whereas under WL both IL46 and IL20 exhibited similar A (25.35 and $24.26 \mu\text{mol m}^{-2} \text{s}^{-1}$, respectively), which was significantly higher than Svevo ($22.66 \mu\text{mol m}^{-2} \text{s}^{-1}$; $P < 0.047$; Supplemental Figure S9). IL20 also maintained significantly higher stomatal conductance (g_s ; $P = 0.013$) and transpiration rate (E ; $P = 0.024$) under WL relative to Svevo (Supplemental Figure S10 and Supplemental Table S5). Under WW treatment, both IL20 and IL46 had higher g_s compared to Svevo.

IL20 exhibits a higher root-to-shoot ratio under water stress

Since IL20 maintained a higher assimilation rate and stomatal conductance under WL treatment, we investigated if this was related to improved water uptake due to the differential root growth response under water stress (Figure 5A). Characterization of soil-grown plant roots (22 DAT) showed that both IL46 and IL20 exhibited higher root biomass relative to Svevo ($P \leq 0.001$) under WW treatment; however, under WL treatment, Svevo root biomass was significantly lower than IL20 ($P = 0.003$, t test). Further, IL20 also exhibited a higher root-to-shoot ratio when compared with Svevo under WL treatment ($P = 0.046$; Figure 5, B and C; Supplemental Table S6). To explore the differential root response of IL20 compared with Svevo in a developmental context, we performed a paper roll seedling assay (Placido et al., 2013). While the shoot length of IL20 and Svevo was similar under WW and WL treatments, IL20 exhibited significantly higher root length throughout the experiment, with 10.3% longer roots at the end of the experiment (25.21 versus 22.85 cm, for IL20 and Svevo, respectively; $P = 0.006$, t test) under WL. This advantage was expressed in the higher (12.5%) root-to-shoot ratio of IL20 compared with Svevo on the last day ($P = 0.001$; Supplemental Figure S11, A–F). This suggests that the root growth dynamic of IL20 is different from Svevo even during the early seedling stage (11 in Zadoks scale) and more apparent under WL treatment, resulting in an increase in the root-to-shoot ratio. These results show that root biomass in later stages (19 in Zadoks scale) and root length at the seedling stage have a

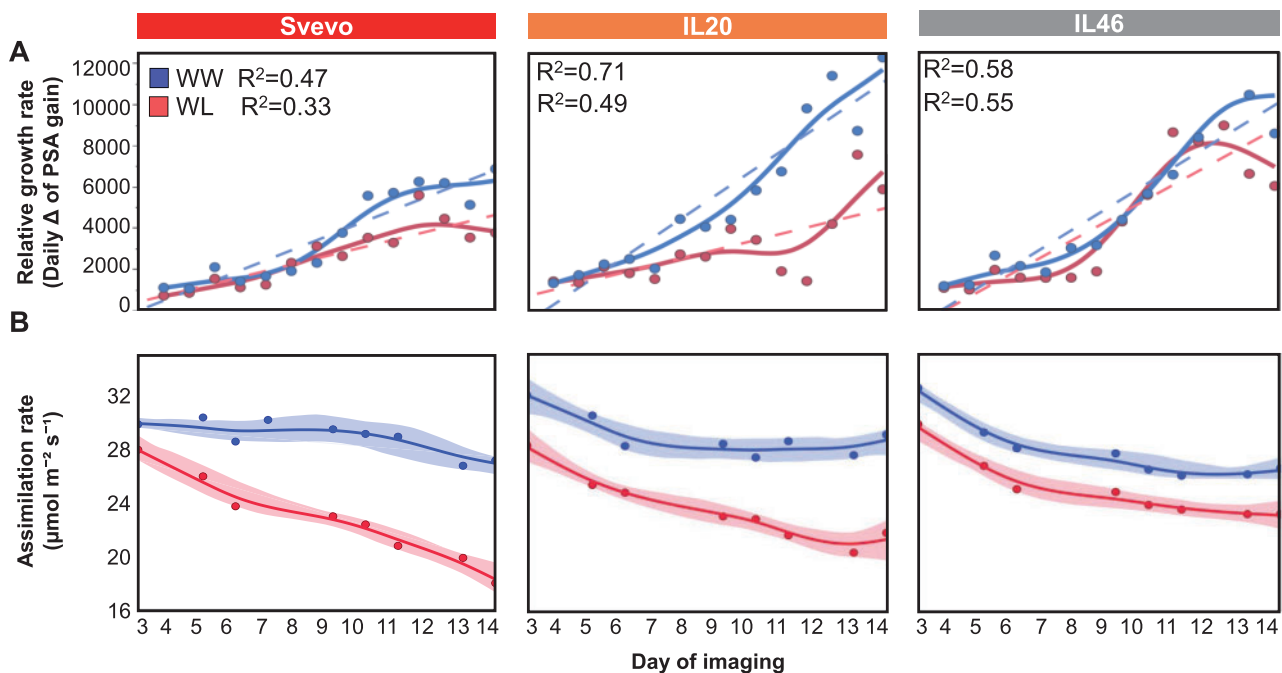


Figure 4 Temporal growth and carbon assimilation dynamics. Time series dynamics of Svevo, IL20, and IL46 for (A) relative growth rate and (B) net assimilation rate under WW (blue) and WL (red) treatments. Dashed lines represent the fitted linear growth of each genotype under specific water treatment. Markers represent the genotypic mean under specific water treatment ($n = 4$). The continuous line represents the smooth curve through the data and the shaded area represents the standard error of the smooth curve.

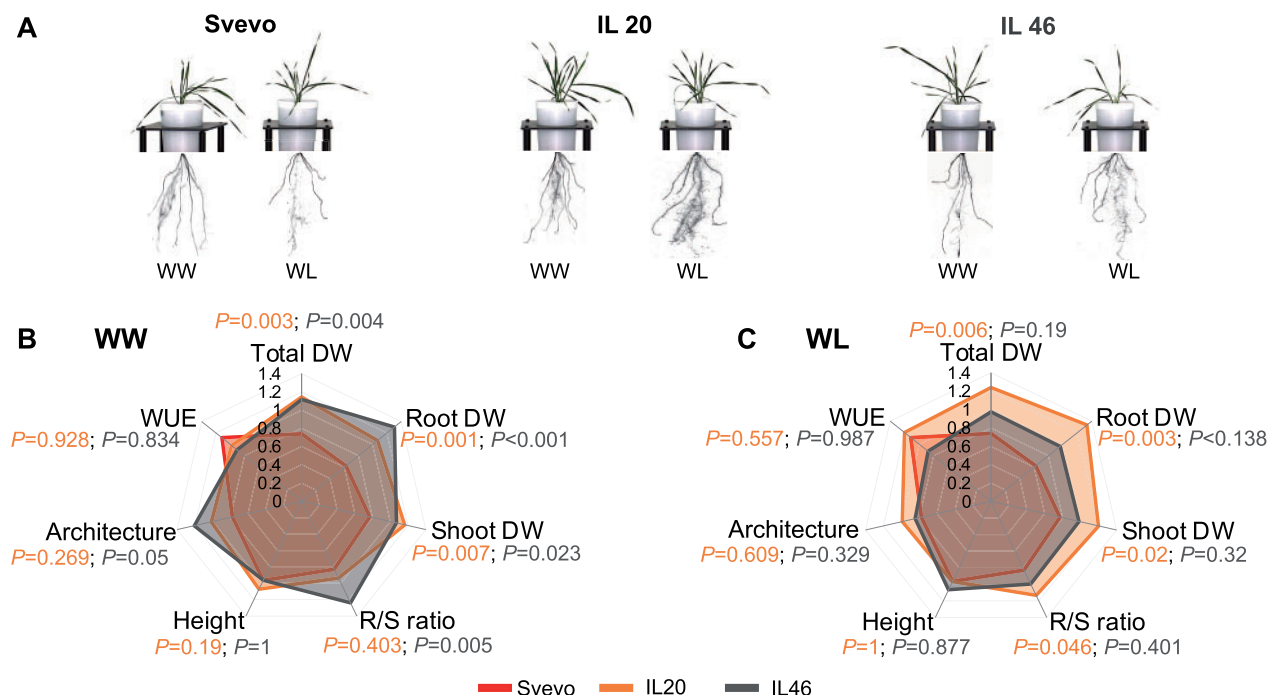


Figure 5 Morpho-physiological modification in response to water stress. A, Representative image of Svevo, IL20, and IL46 under WW and WL treatments 14 d after transplanting. Radar charts comparing the phenotypic traits of Svevo (red), IL20 (orange), and IL46 (gray) plants under (B) WW, and (C) WL treatments. Values are means (P -values were calculated using t tests; $n = 4$). Total dry weight (Total DW), WUE, plant architecture (Architecture), plant height (Height), root-to-shoot ratio (R/S ratio), shoot DW, and root DW.

similar response in IL20 under WL treatment (Figure 5; Supplemental Figure S11).

Root transcriptome analysis identifies genes that colocalize to the introgressions

Given the differential root growth and the root-to-shoot ratio between Svevo and IL20 in the seedling stage, we reasoned that the underlying gene(s) responsible for these phenotypes could be the same, resulting in similar root-to-shoot ratio plasticity that was observed in later vegetative stages. We performed a transcriptome analysis on roots from the seedling stage experiment to identify CGs that underlie the root-to-shoot plasticity phenotype. Seedling root sampling for transcriptome analysis is more precise as it limits gene transcript changes caused by root damage that occurs with sampling roots from older plants growing in soil or sand. We combined transcriptome analysis with the genotypic data of IL20 and Svevo to map the differentially expressed genes (DEGs) to specific introgressions. IL20 has six introgressions from Zavitan, the wild emmer parent, distributed on five chromosomes (Supplemental Table S7), accounting for ~4.5% of the Zavitan genome (Avni et al., 2017). Based on public annotations, a total of 651 genes from the homozygous regions (Supplemental Table S8) map to these introgressions. We identified 599 DEGs in a four-way analysis of genotypic response to WL and differences between genotype under specific water treatment (Figure 6A), of which 425 genes were downregulated and 174 genes were upregulated (Supplemental Table S9).

Notably, 33.4% of the DEGs were found differentially expressed in IL20 in response to WL. In contrast, only 10% of the total DEGs were responsive to WL in Svevo. About 28% of the total DEGs were differentially regulated between Svevo and IL20 under WL, with 37 of these genes resolving to the introgressed segment in IL20.

CGs associated with longer roots under water stress

We next examined the differentially abundant transcript(s) that localize to the introgressions in IL20 and identified 17 DEGs under WW and 18 DEGs under WL treatments between IL20 and Svevo. Given the IL20 root phenotype, we targeted five root-related candidate DEGs (CG; Supplemental Table S10). The criteria used to filter these five genes were based on literature searches of putative orthologs with root-associated phenotypes. Three of these genes were upregulated in IL20 under WL (TRIDC4AG046080, TRIDC4AG048600, and TRIDC2AG073520), one gene was downregulated under WL (TRIDC4AG046660) and one gene (TRIDC4AG046110) showed upregulation under WW treatment only. Of these five genes, TRIDC4AG046080 is a low confidence gene based on annotation of the Zavitan genome. The remaining four genes have an SNP (TRIDC2AG073520, TRIDC4AG048600), carry multiple polymorphisms (TRIDC4AG046660), or have presence/absence variation between the Zavitan and Svevo genomes (TRIDC4AG046110; Supplemental Table S10). TRIDC4AG046110 encodes a *FAR1-RELATED SEQUENCE 4-like* isoform that is downregulated in salt-susceptible sweet sorghum (*Sorghum bicolor*) roots (Yang et al., 2018).

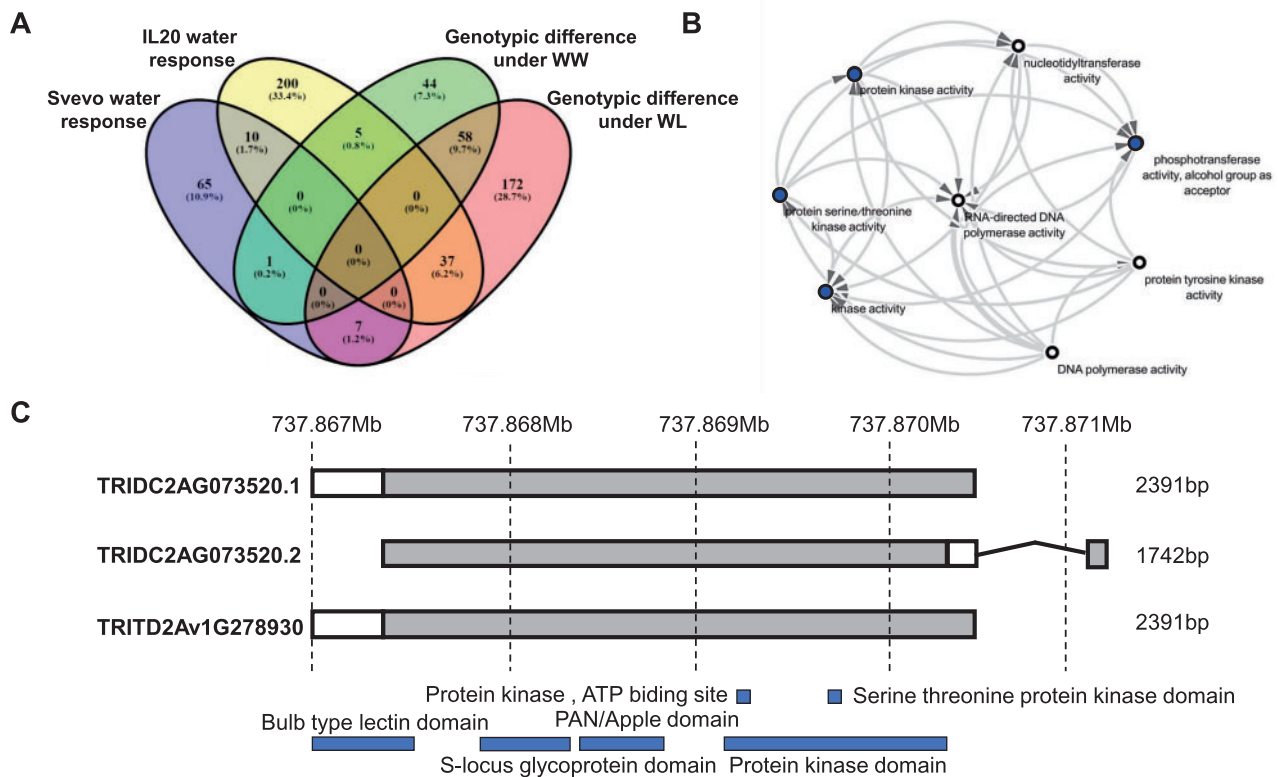


Figure 6 DEGs comparison for IL20 and Svevo. **A**, A four-way Venn diagram of DEGs among IL20 and Svevo under WW and WL treatments. **B**, Network co-expression pattern of the DEGs associated with kinase activity. Nodes with blue color represent higher interaction. **C**, Splice variation of TRIDC2AG073520 gene, a candidate for root phenotypes of IL20 that maps to the introgression. TRITD2Av1G278930 represent the Svevo allele.

TRIDC4AG048600 is a *SIMILAR TO RCD ONE 1 (SRO1)* gene. In *Arabidopsis* (*Arabidopsis thaliana*), a double mutant of *AtSRO1* exhibited shorter roots and a smaller cell division zone compared to wild-type plants (Teotia and Lamb, 2011). Sequence alignment of this gene against the Zavitan genome indicates a truncated protein in the Zavitan genome that may result in loss of function or a modified function.

The remaining three DEGs were associated with protein kinase function (Supplementary Table S10), where network analysis of molecular functions showed significant downstream transferase activity elements in various kinase activities (Figure 6B). TRIDC4AG046080 is a homolog of a rice domain of an unknown function (*DUF581*) that, in *Arabidopsis*, was found to play a role in sucrose non-fermenting-related kinase (*SnRK1*; Nietzsche et al., 2016). TRIDC4AG046660 is a Leucine-rich repeat receptor-like protein kinase (LRR-RLK) and TRIDC2AG073520 is a G-type lectin S-receptor-like serine/threonine-protein kinase (RLK). We examined the sequence of TRIDC2AG073520 in the Zavitan genome (Avni et al., 2017) and identified two splice variants on chromosome 2A that are 2391 bp and 1742 bp for TRIDC2AG073520.1 and TRIDC2AG073520.2, respectively. In contrast, only a single variant (2391 bp) was found in durum wheat (*cv* Svevo; Figure 6C) as well as among 10 hexaploid bread wheat cultivar genomes (Appels et al., 2018; Walkowiak et al., 2020). In the tissue-specific gene expression atlas of Zavitan, this gene has the highest expression in

roots with almost no reads detected in other tissues. The combination of splicing variation difference between Zavitan and cultivated wheat and the specificity of root expression suggests that TRIDC2AG073520 is a strong CG underlying the root-to-shoot ratio difference exhibited by IL20 (Supplemental Figure S12).

Discussion

Wild plants have developed various reversible and nonreversible phenotypic plasticity strategies to cope with environmental uncertainty. Selection by humans, often under less variable environmental conditions, has likely resulted in higher crop-plant phenotypic stability (Lopes et al., 2015). Consequently, many modern cultivars may have lost some of the fitness components needed for adapting to climate-driven variation in many regions (Kissoudis et al., 2016). Our work shows that the introgression of Zavitan alleles into a modern durum cultivar promoted higher phenotypic diversity, as expressed in plant architecture and biomass accumulation at vegetative stage (Figure 1). The IL panel was developed from a single wild emmer accession (Zavitan), yet it resulted in wide segregation of morpho-physiological traits (either positively or negatively). This accession originated from a habitat with high soil moisture fluctuations due to a shallow brown basaltic soil type, which has been shown to promote diversity (Peleg et al., 2008). The phenotypic variation observed in this study is reflective of the quantitative

nature of these traits and the different combinations of wild and domesticated alleles. Interestingly, the mean biomass accumulation trajectory over time of the IL panel was similar to Svevo under both water treatments.

Water stress reduced biomass by around 50% (i.e. PSA) and altered plant architecture (i.e. convex area 12.5%–48.5%) relative to the WW treatment (Supplemental Figure S3), with both variables being positively associated with one another (Figure 1). Increased phenotypic variation in response to water stress was quantified by calculation of the drought susceptibility index (S-index). The combination of IL performance under WL with their S-indexes resulted in five distinct clusters of high phenotypic stability (HPS, LPS) and phenotypic plasticity (HPP, MP, LP). Phenotypic stability is often associated with small changes in plant performance in response to unfavorable conditions. Escape (i.e. completing a rapid life-cycle to avoid the stress) is a common strategy of wild plants in xeric habitats and has been repeatedly reported for many wild grasses such as wild emmer (Peleg et al., 2005), *Brachypodium distachyon* (Opanowicz et al., 2008), and *Avena barbata* (Sherrard and Maherali, 2006). Accordingly, the two clusters exhibiting phenotypic stability had biomass reductions of only 45% and 40% for LPS and HPS, respectively. Interestingly, the LPS had characteristics of “small plants” (PSA, 50.4, and 27.8 kPixel for WW and WL, respectively), whereas HPS had high biomass under WW and the highest values among all clusters under WL (67.1 and 40.6 kPixel, respectively). These results suggest that the phenotypic stability strategy is not size-dependent, but rather an active mechanism that enables plants to cope with water stress.

Temporal characterization of the responsiveness clusters showed that clusters with high phenotypic plasticity responded earlier (12, 8, and 10 kPixel for LP, MP, and HPP, respectively) than those in high stability clusters (20 and 26 kPixel for LPS and HPS, respectively; Figure 3A). To understand the temporal genetic architecture of the responsiveness clusters, we calculated broad-sense heritability ($b_s h^2$) dynamics. While the plasticity clusters exhibited a decrease in PSA $b_s h^2$ over time as a consequence of high $G \times E$ interaction ($\sigma^2_{G \times E}$) and low genetic component (σ^2_G), the more phenotypically stable clusters showed increased heritability during early growth and decreased heritability at later stages, which corresponded to the late stress responses (Figure 3).

The two high productivity clusters (HPS and HPP) exhibited contrasting response mechanisms, with the plasticity cluster responding earlier (16, 17, and 8 d for PSA, plant density, and plant architecture, respectively; Figure 3; Supplemental Figure S7). Detailed characterization of representative accessions for these two clusters (represented by IL20 and IL46 for HPP and HPS, respectively) suggests a size-independent response to water stress. Consistent with the growth phenotype, IL46 maintained similar photosynthetic and transpiration rates under WW and WL, while IL20 responded as early as day 12, limiting its assimilation

rate. Notably, IL20 had the highest photosynthetic rate under WW and exhibited a larger reduction under WL yet was able to maintain a significantly higher assimilation rate than Svevo.

In this work, we focused on downstream genetic characterization of the highly plastic response represented by IL20. Our rationale for this prioritization was to elucidate the mechanisms that can enable plants to alter carbon allocation (between root and shoot) in response to water limitations as a more viable strategy for cereals during vegetative growth stage. Notably, IL20 had the highest photosynthetic rate under WW among the three genotypes assayed and exhibited a larger reduction under WL, yet was able to maintain a significantly higher assimilation rate than Svevo. Further, the size and number of introgressions in IL20 relative to IL46 made it more tractable for initial molecular characterization.

Fast stress responsiveness strategy (IL20 strategy) may negatively affect carbon assimilation and growth; on the other hand, early acclimation can trigger a metabolic shift of carbon allocation to different plant organs (Rodrigues et al., 1993; Bohnert and Sheveleva, 1998). Thus, under water limitation, root-to-shoot ratio plasticity can mediate optimal resource partitioning between growth and development (Voss-Fels et al., 2017). Modern bread wheat cultivars have lower root-to-shoot ratios as compared to landraces (Siddique et al., 1990). Moreover, a comparison among wild emmer, domesticated emmer, and durum wheat showed a trend of reduced root-to-shoot ratio during the initial domestication from wild to domesticated emmer, and during wheat evolution under domestication (Gioia et al., 2015; Roucou et al., 2018). Accordingly, the introgression of alleles from Zavitan in the background of the elite durum wheat cultivar significantly increased the root-to-shoot ratio (30%) under WL as compared with the parental line (Figure 5C). Likewise, Merchuk-Ovnat et al. (2017) reported a higher root-to-shoot ratio in response to water stress from wild emmer (*acc.* G18-16) introgression in the background of elite bread wheat cultivars. Thus, introducing new genetic diversity for root-to-shoot ratio plasticity from wild progenitors could facilitate the resilience of modern wheat cultivars to the projected fluctuating water availability during the growing season.

The root system is the site of interactions with the rhizosphere; thus, root architectural plasticity (i.e. resource allocation, morphological, anatomical, or developmental) is a critical adaptation strategy to environmental cues (Rellán-Álvarez et al., 2016; Golan et al., 2018). To better understand the genetic mechanism associated with the increased root biomass of IL20, we analyzed the transcriptome response of roots under water stress. In general, the differential transcriptional response of IL20 to WL was greater than Svevo (242 versus 73 DEGs, respectively). We estimate that IL20 has ~4.5% of the Zavitan genome and ~6% of the DEGs colocalize to these introgressed segments. This proportionate alien genomic and differential transcriptomic

constitution under WL suggests that the trans-regulation of the transcriptome response due to introgressions dominates the cis-transcriptional responses originating from the introgressions. This higher degree of transcriptional response (higher DEGs) due to wild introgressions could be due to greater genetic variation resulting in greater phenotypic plasticity compared to the domesticated germplasm. This in part could be driven by greater environmental sensitivity of wild alleles of signaling genes or/and transcription factors localized to the introgressions.

Downstream gene network analysis highlighted the key role of protein kinases as hubs of interaction (Figure 6B). Three CGs (TRIDC4AG046080, TRIDC2AG073520, and TRIDC4AG046660) were found associated with protein kinase function that mediates plant hormone and nutrient signaling, and cell cycle regulation (Laurie and Halford, 2001; Virlet et al., 2017). TRIDC4AG046660 is a LRR-RLK. Mutants of this gene in Arabidopsis (*At2g33170*) control root growth and are mediated by cytokinin (ten Hove et al., 2011). TRIDC4AG046080 (DUF581 in rice) interacts with *SnRK1* and is regulated by hormones and differentially regulated by hormones and environmental signals (Nietzsche et al., 2016). Wheat mutants containing a conserved DUF581 domain revealed a salt-induced gene (TaSRHP). Early stages of salt stress typically have an osmotic stress component that is similar to water stress. The overexpression of this gene in wild-type Arabidopsis resulted in enhanced resistance to both salt and drought stresses (Hou et al., 2013).

TRIDC2AG073520 (TRITD2Av1G27893 in Svevo) is a G-type lectin S-receptor-like serine/threonine-protein kinase gene. The domesticated allele contains a nonsynonymous mutation expressed as an amino acid shift (isoleucine to threonine). This CG was significantly upregulated under WL in IL20 (FC 2.29, $P_{\text{adj}}=0.03$). In Arabidopsis, drought and salinity stress induced upregulation of the gene (Sun et al., 2013). Moreover, the gene was expressed specifically in root tissue from the early seedling stage to 50% of ear emergence (Supplemental Figure S13; Ramírez-González et al., 2018). Genetic dissection showed that the genomic region of this gene overlaps with a Quantitative Trait Loci (QTL) affecting lateral root number per primary root (Maccaferri et al., 2016).

Two splice variants of TRITD2Av1G278930 were identified in the wild emmer genome (TRIDC2AG073520.1 and TRIDC2AG073520.2) and these included several polymorphisms in each variant. The TRIDC2AG073520.1 variant is similar to the domesticated variant, although it contains a nonsynonymous SNP. This gene was compared to the wheat pan-genome (Walkowiak et al., 2020) and a similar SNP was found in all genomes compared to Zavitan, suggesting variation between wild and domesticated wheats. The TRIDC2AG073520.2 variant is different in length and exon number; however, the domains remain similar to the domesticated variant and the additional exon does not encode for a specific known domain (Figure 6C). The underlying mechanisms by which the identified splice variance and/or

amino acid substitution affect wild emmer response to stress via longer root systems are yet to be discovered.

Concluding remarks and future perspective

In this study, we show that targeting small and hence more genetically tractable wild introgressions can yield surprisingly divergent phenotypic responses to water stress even with prior selection of ILs for agronomically viable phenology. Our detailed physiological characterization combined with a temporal phenomics approach provides insights into the divergent water stress response dynamics in an elite durum background. The results reported and those that will be studied in additional ILs can result in a new set of alleles and CG resources to enhance drought adaptation in durum wheat. Further, genetic elucidation of drought adaptive phenotypic plasticity can inform similar studies in bread wheat and other cereals due to high incidence of conserved gene function and synteny. Collectively, our results suggest that incorporating the wild gene/alleles can enable greater phenotypic plasticity and has the potential to enhance environmental stress resilience.

Material and methods

Plant material and experimental design

The wild emmer (*T. turgidum* ssp. *dicoccoides*) accession Zavitan was selected as a donor for the current study based on its robust morphology and drought tolerance characteristics (Supplemental Figure S1). A recombinant inbred line population derived from a cross between durum wheat (*cv* Svevo) and wild emmer (*acc.* Zavitan) was previously developed (Avni et al., 2014). Adapted RILs, i.e. with the genetic composition of post-domestication alleles of dwarfing gene *Reduce height (Rht)-B1b* and nonbrittle spike genes (*TtBtr1-A* and *TtBtr1-B*), were backcrossed three-times and selfed over three generations (described in detail in Oren, 2020). The 47 ILs were genotyped (Infinium iSelect 90K SNP chip array), resulting in equal SNP distribution across the genomes. Detailed information for the ILs panel is provided in Supplementary Table S11 and raw genotyped data are available (<https://data.mendeley.com/datasets/4vb99xs659/1>).

Uniform seeds of 47 ILs and their recurrent parent were used for the current study. Seeds were surface disinfected (1% (v/v) sodium hypochloric acid for 30 min) and placed on moist germination paper (Anchor Paper Co., St Paul, MN, USA) at 24°C in the dark for 5 d. Uniform seedlings were transplanted to pots (2L, 45 × 19.5 cm) filled with 1.2 kg of Fafard germination soil (Sungro, MA, USA), and were thinned to one plant per pot 6 DAT. Pots were placed on automated carriers in the greenhouse (22°C/16°C day/night) and watered daily to 80% FC. The experiment started at 11 DAT (2–4 in Zadoks scale; Zadoks et al., 1974) and continued until the tillering stage (Zadoks 29–33). Greenhouse temperature was kept at 22°C/16°C (day/night) during the experiment. The daytime photosynthetically active radiation was supplemented with LED red/blue light lamps, with an intensity of 200 $\mu\text{mol m}^{-2} \text{s}^{-1}$. The experiment was

conducted at the Nebraska Innovation Campus greenhouse high-throughput plant phenotyping core facility (Scanalyzer 3D, LemnaTec GmbH, Aachen, Germany), University of Nebraska-Lincoln.

A two-way factorial complete randomized experimental design, with 47 ILs and the recurrent parent, Svevo, was conducted. Two water treatments were applied: well-watered (control, WW) at 80% FC and WL at 30% FC (Supplemental Figure S14), with three replicates for each combination (288 pots total). Plants were imaged daily for 35 d with visible red, green, and blue (RGB) camera (Basler, Ahrensburg, Germany) taking five side-views (rotating 72°) and a single top-view. The image size was 2,454 × 2,056 pixels. After imaging, each pot was automatically weighed and watered to meet its calculated target weight.

Based on the results of the first experiment, we selected two ILs representing the most productive clusters under WL treatment: IL20 from the high plasticity cluster (HHPH) and IL46 from the high stability cluster (HPSH). A two-way factorial complete randomized design was conducted, with three genotypes and two water treatments as described above, with four replicates for a total of 24 pots. The imaging started seven DAT and imaging continued for 14 d. Plants were characterized for gas exchange from 9 to 20 DAT and root biomass was harvested at the end of the experiment (21 DAT).

Image processing and trait characterization

Phenolmage GUI software was used for image processing (Zhu et al., 2021). All raw RGB images were deposited in the CyVerse and can be accessed at <https://doi.org/10.25739/ezt-p-dj42>. We extracted some key morphological traits derived from RGB images, including PSA, plant height and width, plant architecture (convex area), plant density, and WUE on the final day of the experiment. *Plant height* and *plant width* were calculated from plant dimensions. *Plant architecture* (convex area) was calculated to predict plant architecture trajectory. *Density* was calculated based on the ratio between pixel sum and plant architecture. On the last day of the experiment, a subset of 18 ILs were harvested, oven-dried (80°C), and weighed to obtain shoot dry weight. Correlation analysis showed a high correlation between PSA and shoot dry weight ($r = 0.96$; $P < 10^{-4}$; Supplemental Figure S2). The *relative growth rate* was calculated by dividing daily pixel accumulation with pixel numbers from the previous day. Daily WUE_t was calculated as described by Momen et al. (2019), where (t) represents the day.

$$WUE_t = \frac{\Delta PSA(\text{Pixels})}{\Delta WU(\text{ml})}$$

where ΔPSA is the daily PSA:

$$\Delta PSA = PSA_{t-1} - PSA_t$$

and ΔWU is the daily water used:

$$\Delta WU = \text{Potweight}_{t-1} - \text{Potweight}_t$$

Photosynthetic rate, transpiration rate, and stomatal conductance were measured between 10 and 22 DAT (Zadoks 15–19) using a portable infra-red gas analyzer (LI-6800XT; Li-Cor Inc., Lincoln, NE, USA). Measurements were conducted at the mid-portion of the last fully expanded leaf from 9:00 to 13:00 ($n = 3$).

Root DW was measured at 22 DAT. Root tissue was harvested ($n = 4$), washed and oven-dried (80°C) for 72 h, and weighed to obtain root DW. The root-to-shoot ratio was calculated by dividing root DW by PSA (shoot DW).

Characterization of root and shoot length

Five uniform seeds of Svevo and IL20 were grown on moist germination paper (25 × 38 cm; Anchor Paper Co., St Paul, MN, USA), as previously described (Golan et al., 2018). A two-way factorial design was applied with two genotypes and two water treatments, with eight replicates (total of 32). Eight cigar rolls were placed in a container (4 L) and refilled daily to keep the availability of 100 mL of water. The WL treatment container was filled once with 20 mL of water and was not re-filled during the experiment. Each container was wrapped with plastic to prevent water evaporation. Shoot and root length were measured daily by scale, from 3 to 8 DAT (Zadoks stage 11).

Statistical analyses

The JMP ver. 15 statistical package (SAS Institute, Cary, NC, USA) was used for statistical analyses unless otherwise specified. The temporal response was fitted for genotypes (collectively or separately) under each water treatment. Analysis of variance (ANOVA) was used to assess the possible effects of genotype (G), environment (E), and G × E interactions on morpho-physiological traits of genotypes. Frequency distribution was determined for all morpho-physiological traits on the last day. Components of descriptive statistics are graphically presented in the box plot: median value (horizontal short line), quartile range (25% and 75%), and data range (vertical long line). Pearson correlation for all traits was conducted for each water treatment. An agglomerative hierarchical procedure with an incremental sum of squares grouping strategy was employed using Ward's method. PCA was based on a correlation matrix and is presented as biplot ordinations of the ILs (PC scores). Drought-susceptibility index (S) was calculated based on Peleg et al. (2005):

$$S = \frac{1 - Y_{WL}/Y_{WW}}{1 - X_{WL}/X_{WW}}$$

where Y_{WL} and Y_{WW} are the mean phenotypic values of a certain genotype under the respective treatments, and X_{WL} and X_{WW} are the mean performances of all genotypes. Density distribution conducted using ggplot packages and stability of the cluster was tested using the clusterboot (fpc) package (R Core Team, 2021).

Broad-sense heritability dynamics

Broad-sense heritability (h^2) and its components, genetic component (σ_g^2), and $G \times E$ interaction ($\sigma_{g \times e}^2$) were calculated for each day of imaging across the two water treatments using ANOVA-based variance components: $h^2 = \sigma_g^2 / \sigma_g^2 + \sigma_{g \times e}^2 / e$, where $\sigma_g^2 = [(MS_{IL} - MS_{IL \times e}) / e]$, $\sigma_{g \times e}^2 = MS_{IL \times e}$, e is the number of water treatments and MS is the mean square.

RNA extraction and sequencing

Based on the physiological analysis, we collected root tissues six days after germination (Zadoks 11) for RNAseq ($n = 2$) and froze them in liquid nitrogen. RNA was extracted using the plant/fungi total RNA purification kit (Norgen Biotek Corp., Canada) with on-column DNase treatment (Qiagen, Germany). Sample contamination and RNA integrity were assessed using the Nan D-1000 spectrophotometer (Thermo Fisher Scientific). Single-end (150 bp) bar-coded cDNA libraries were prepared for sequencing on the Illumina HiSeq2000 sequencer (NGS Core, Nebraska Medical Center, Omaha, USA).

Data processing and analysis

FastQ quality of each sample was manually inspected using FastQC (<http://www.bioinformatics.babraham.ac.uk/projects/fastqc>). Barcode removal, filtering, and trimming of low-quality reads were executed using the command line tool Trimmomatic. Each RNA-seq read was trimmed to make sure the average quality score exceeded 30 and had a minimum length of 70 bp. Sequences were aligned to the available Svevo and Zavitan reference genomes (Avni et al., 2017; Maccaferri et al., 2019) using TopHat (Trapnell et al., 2009). Numbers of reads per gene were counted by the software tool of HTSeq-count using corresponding rice gene annotations and the “union” resolution mode (<http://www-huber.embl.de/users/anders/HTSeq>). Differential expression analysis of count data and data visualization was conducted with the DESeq2 package (Love et al., 2014). To detect significant DEGs, a 5% false discovery rate correction for multiple comparisons was determined (Benjamini and Hochberg, 1995), and a minimal $|0.5| \log_2 FC$ threshold was applied. Venn diagrams were created with <http://bioinformatics.psb.ugent.be/webtools/Venn>. Gene ontology (GO), singular enrichment analysis, and parametric analysis of DEG set enrichment for biological processes and pathways were conducted with AgriGO (<http://systemsbiology.cau.edu.cn/agriGOv2>).

GO and CGs analysis

Biological processes and molecular function networks were established using all the filtered DEGs for GO terms with REVIGO software (<http://revigo.irb.hr>) with a clustering algorithm and the outputs were transferred to the Cytoscape software (<https://cytoscape.org>).

CGs were analyzed on the wheat efp browser for expression in different tissues and phenological stages (http://bar.utoronto.ca/efp_wheat/cgi-bin/efpWeb.cgi). Gene sequences were compared with genomes of Svevo ([\[usda.gov/GG3/genome_browser\]\(https://wheat.pw.usda.gov/GG3/genome_browser\)\) and Zavitan \(\[https://wheat.pw.usda.gov/cgi-bin/seqserve/blast_wheat.cgi\]\(https://wheat.pw.usda.gov/cgi-bin/seqserve/blast_wheat.cgi\)\). Differences in splice variance of CGs were perceived from the blast on GrainGenes \(\[https://wheat.pw.usda.gov/cgi-bin/seqserve/blast_wheat.cgi\]\(https://wheat.pw.usda.gov/cgi-bin/seqserve/blast_wheat.cgi\)\). DNA translation to amino acids was done with expasy \(<https://web.expasy.org/translate>\).](https://wheat.pw.</p>
</div>
<div data-bbox=)

Accession number

Raw sequencing files of mRNA sequencing are available at the short read archive of the National Center for Biotechnology Information (<https://www.ncbi.nlm.nih.gov>) under accession number GSE163450. Major genes referenced in the main text are provided in Supplemental Tables S9 and S10.

Supplemental data

The following materials are available in the online version of this article.

Supplemental Table S1. Correlations between morpho-physiological traits under WW and WL treatments.

Supplemental Table S2. Temporal coefficient of variance for PSA.

Supplemental Table S3. Comparison of PSA, plant architecture, and plant architecture density under two water treatments for each cluster.

Supplemental Table S4. Regression equation of relative growth rate.

Supplemental Table S5. Comparisons of A, T, and G_s among Svevo, IL20, and IL46 under two water treatments throughout the experiment.

Supplemental Table S6. Comparisons of morpho-physiological traits among Svevo, IL20, and IL46 under two water treatments.

Supplemental Table S7. The physical location of wild emmer introgressions of IL20 on the Zavitan genome.

Supplemental Table S8. Gene annotation within IL20 introgressions.

Supplemental Table S9. Significant DEGs.

Supplemental Table S10. Root-related CGs.

Supplemental Table S11. List of ILs and their chromosomal introgressions.

Supplemental Figure S1. Physiological differences between the population parents under WW and WL treatments.

Supplemental Figure S2. Correlation between projected shoot area and shoot dry weight.

Supplemental Figure S3. Time series dynamics of morpho-physiological traits under contrasting water treatment.

Supplemental Figure S4. Plant projected shoot area dynamics of ILs and Svevo under WW and WL treatments.

Supplemental Figure S5. S-index distributions of morpho-physiological traits under WW and WL treatments.

Supplemental Figure S6. Principal component analysis of morpho-physiological traits.

Supplemental Figure S7. Time series dynamic of plant architecture and density.

Supplemental Figure S8. Time series heritability dynamics of plant density and architecture.

Supplemental Figure S9. Time series dynamics of Svevo, IL20, and IL46 assimilation rate under WW and WL treatments.

Supplemental Figure S10. Time series dynamics for stomatal conductance and transpiration rate under WW and WL treatments.

Supplemental Figure S11. Time series dynamics of the root-to-shoot ratio under contrasting water treatment.

Supplemental Figure S12. Heat map of CGs from Zavitan expression atlas and read count of the CG TRIDC2AG073520 at different developmental stages.

Supplemental Figure S13. Expression atlas of TRIDC2AG073520 in the wheat efp browser.

Supplemental Figure S14. Experimental design.

Acknowledgments

We thank members of the Peleg and Walia labs for technical assistance with experiments. We thank Dr Paul Staswick for critically reading the manuscript.

Funding

This research was partially supported by the Chief Scientist of the Israel Ministry of Agriculture and Rural Development, US Agency for International Development Middle East Research and Cooperation (grant #M34-037) to Z.P., and the Agricultural Research Division Wheat Innovation Fund from the University of Nebraska-Lincoln to H.W. and T.A.

Conflict of interest statement. None declared.

References

- Appels R, Eversole K, Feuillet C, Keller B, Singh K, Chhuneja P, Gupta OP, Jindal S, Kaur P, Malik P, et al.** (2018) Shifting the limits in wheat research and breeding using a fully annotated reference genome. *Science* **361**: eaar7191.
- Araus JL, Slafer GA, Reynolds MP, Royo C** (2002) Plant breeding and drought in C₃ cereals: what should we breed for? *Ann Bot* **7**: 925–940
- Ashley DA, Boerma HR** (1989) Canopy photosynthesis and its association with seed yield in advanced generations of a soybean cross. *Crop Sci* **29**: 1042–1045
- Avni R, Nave M, Barad O, Baruch K, Twardziok SO, Gundlach H, Hale I, Mascher M, Spannagl M, Wiebe K, et al.** (2017) Wild emmer genome architecture and diversity elucidate wheat evolution and domestication. *Science* **357**: 93–97
- Avni R, Nave M, Eilam T, Sela H, Alekperov C, Peleg Z, Dvorak J, Korol A, Distelfeld A** (2014) Ultra-dense genetic map of durum wheat × wild emmer wheat developed using the 90K iSelect SNP genotyping assay. *Mol Breed* **34**: 1549–1562
- Benjamini Y, Hochberg Y** (1995) Controlling the false discovery rate: A practical and powerful approach to multiple testing. *J R Stat Soc Ser B* **57**: 289–300
- Bohnert HJ, Sheveleva E** (1998) Plant stress adaptations-making metabolism move. *Curr Opin Plant Biol* **1**: 267–274
- Bradshaw AD** (2006) Unravelling phenotypic plasticity – why should we bother? *New Phytol* **170**: 644–648
- Campos H, Cooper M, Habben JE, Edmeades GO, Schussler JR** (2004) Improving drought tolerance in maize: a view from industry. *Field Crops Res* **90**: 19–34
- Chevin LM, Lande R, Mace GM** (2010) Adaptation, plasticity, and extinction in a changing environment: Towards a predictive theory. *Plos Biol* **8**: e1000357
- Correa J, Postma JA, Watt M, Wojciechowski T** (2019) Soil compaction and the architectural plasticity of root systems. *J Exp Bot* **70**: 6019–6034
- Fragley N, Evans G, Biernaskie JM, Cockram J, Marr EC, Oliver AG, Ober E, Jones H** (2020) Effects of breeding history and crop management on the root architecture of wheat. *Plant Soil* **452**: 587–600
- Fuerst-Bjeliš B** (2017) Mediterranean identities: environment, society, culture. BoD–Books on Demand.
- Furbank RT, Tester M** (2011) Phenomics - technologies to relieve the phenotyping bottleneck. *Trends Plant Sci* **16**: 635–644
- Gioia T, Nagel KA, Beleggia R, Fragasso M, Ficco DBM, Pieruschka R, De Vita P, Fiorani F, Papa R** (2015) Impact of domestication on the phenotypic architecture of durum wheat under contrasting nitrogen fertilization. *J Exp Bot* **66**: 5519–5530
- Golan G, Hendel E, Méndez Espitia GE, Schwartz N, Peleg Z** (2018) Activation of seminal root primordia during wheat domestication reveals underlying mechanisms of plant resilience. *Plant Cell Environ* **41**: 755–766
- Hendel E, Bacher H, Oksenberg A, Walia H, Schwartz N, Peleg Z** (2021) Deciphering the genetic basis of wheat seminal root anatomy uncovers ancestral axial conductance alleles. *Plant Cell Environ* **44**: 1921–1934
- Hennig C** (2008) Dissolution point and isolation robustness: robustness criteria for general cluster analysis methods. *Multivar J* **99**: 1154–1176
- Hou X, Liang Y, He X, Shen Y, Huang Z** (2013) A novel ABA-responsive TaSRHP Gene from wheat contributes to enhanced resistance to salt stress in *Arabidopsis thaliana*. *Plant Mol Biol Rep* **31**: 791–801
- Jin X, Zarco-Tejada PJ, Schmidhalter U, Reynolds MP, Hawkesford MJ, Varshney RK, Yang T, Nie C, Li Z, Ming B, et al.** (2021) High-throughput estimation of crop traits. *IEEE Geosci Remote Sens Mag* **9**: 200–231
- Jump AS, Marchant R, Peñuelas J** (2009) Environmental change and the option value of genetic diversity. *Trends Plant Sci* **14**: 51–58
- Kara Y, Martin A, Souyris I, Rekika D, Monneveux, P** (2000) Root characteristics in durum wheat (*T. turgidum* conv. durum) and some wild Triticeae species. Genetic variation and relationship with plant architecture. *Cereal Res Commun* **28**: 247–254
- Kirkegaard JA, Lilley JM, Graham JM** (2007) Impact of subsoil water use on wheat yield. *J Agric Res* **58**: 303–315
- Kissoudis C, van de Wiel C, Visser RGF, van der Linden G** (2016) Future-proof crops: challenges and strategies for climate resilience improvement. *Curr Opin Plant Biol* **30**: 47–56
- Lambers H, Atkin OK, Millenaar FF** (2002) Respiratory patterns in roots in relation to their functioning. In Y Waisel, A Eshel, U Kafkaki, eds, *Plant Roots: The Hidden Half*, Ed 4. Marcel Dekker, Inc., New York, NY, pp 521–552
- Langridge P, Reynolds M** (2021) Breeding for drought and heat tolerance in wheat. *Theor Appl Genet*. DOI: 10.1007/s00122-021-03795-1.
- Laurie S, Halford NG** (2001) The role of protein kinases in the regulation of plant growth and development. *Plant Growth Regul* **34**: 253–265
- Lopes MS, El-Basyoni I, Baenziger PS, Singh S, Royo C, Ozbek K, Aktas H, Ozer E, Ozdemir F, Manickavelu A, et al.** (2015)

- Exploiting genetic diversity from landraces in wheat breeding for adaptation to climate change. *J Exp Bot* **66**: 3477–3486
- Love MI, Huber W, Anders S** (2014) Moderated estimation of fold change and dispersion for RNA-seq data with DESeq2. *Genome Biol* **15**: 550
- Maccaferri M, El-Feki W, Nazemi G, Salvi S, Canè MA, Colalongo MC, Stefanelli S, Tuberosa R** (2016) Prioritizing quantitative trait loci for root system architecture in tetraploid wheat. *J Exp Bot* **67**: 1161–1178
- Maccaferri M, Harris NS, Twardziok SO, Pasam RK, Gundlach H, Spannagl M, Ormanbekova D, Lux T, Prade VM, Milner SG, et al.** (2019) Durum wheat genome highlights past domestication signatures and future improvement targets. *Nat Genet* **51**: 885–895
- Merchuk-Ovnat L, Fahima T, Ephrath JE, Krugman T, Saranga Y** (2017) Ancestral QTL alleles from wild emmer wheat enhance root development under drought in modern wheat. *Front Plant Sci* **8**: 1–12
- Momen M, Campbell MT, Walia H, Morota G** (2019) Utilizing trait networks and structural equation models as tools to interpret multi-trait genome-wide association studies. *Plant Methods* **15**: 107
- Nietzsche M, Landgraf R, Tohge T, Börnke F** (2016) A protein-protein interaction network linking the energy-sensor kinase SnRK1 to multiple signaling pathways in *Arabidopsis thaliana*. *Curr Plant Biol* **5**: 36–44
- Opanowicz M, Vain P, Draper J, Parker D, Doonan JH** (2008) *Brachypodium distachyon*: making hay with a wild grass. *Trends Plant Sci* **13**: 172–177
- Oren L** (2020) Genetic dissection of polygenic traits from wild emmer wheat using Near isogenic line (NIL) population. M.Sc. Thesis. Tel Aviv University, Tel Aviv, Israel
- Passioura JB, Angus JF.** (2010). Improving productivity of crops in water-limited environments. *Adv Agron* **106**: 37–75
- Pauli D, Chapman SC, Bart R, Topp CN, Lawrence-Dill CJ, Poland J, Gore MA** (2016) The quest for understanding phenotypic variation via integrated approaches in the field environment. *Plant Physiol* **172**: 622–634
- Peleg Z, Fahima T, Abbo S, Krugman T, Nevo E, Yakir D, Saranga Y** (2005) Genetic diversity for drought resistance in wild emmer wheat and its ecogeographical associations. *Plant Cell Environ* **28**: 176–191
- Peleg Z, Saranga Y, Krugman T, Abbo S, Nevo E, Fahima T** (2008) Allelic diversity associated with aridity gradient in wild emmer wheat populations. *Plant Cell Environ* **31**: 39–49
- Placido DF, Campbell MT, Folsom JJ, Cui X, Kruger GR, Baenziger PS, Walia H** (2013) Introgression of novel traits from a wild wheat relative improves drought adaptation in wheat. *Plant Physiol* **161**: 1806–1819
- R Core Team** (2021) R: A Language and Environment for Statistical Computing. R Foundation for Statistical Computing, Vienna, Austria
- Ramírez-González RH, Borrill P, Lang D, Harrington SA, Brinton J, Venturini L, Davey M, Jacobs J, van Ex F, Pasha A, et al.** (2018) The transcriptional landscape of polyploid wheat. *Science* **361**: eaar6089
- Relán-Álvarez R, Lobet G, Dinneny JR** (2016) Environmental control of root system biology. *Annu Rev Plant Biol* **67**: 619–642
- Reynolds MP, Pask AJD, Hoppitt, WJE, Sonder K, Sukumaran S, Molero G, Joshi Arun K** (2017) Strategic crossing of biomass and harvest index source and sink achieves genetic gains in wheat. *Euphytica* **213**: 257
- Rodrigues M, Chaves M, Wendler R, David M, Quick W, Leegood R, Stitt M, Pereira J** (1993) Osmotic adjustment in water stressed grapevine leaves in relation to carbon assimilation. *Funct Plant Biol* **20**: 309–321
- Roucou A, Violle C, Fort F, Roumet P, Ecnartot M, Vile D** (2018) Shifts in plant functional strategies over the course of wheat domestication. *J Appl Ecol* **55**: 25–37
- Royo C, Soriano JM, Álvaro F** (2017). Wheat: a crop in the bottom of the Mediterranean diet pyramid. In B Fuerst-Bjelis, eds, *Mediterranean Identities—Environment, Society, Culture*. Intechopen, London, pp 381–399
- Sayar R, Khemira H, Kharrat M.** 2007. Inheritance of deeper root length and grain yield in half-diallel durum wheat (*Triticum durum*) crosses. *Ann Appl Biol* **151**: 213–220
- Sherrard ME, Maherali H** (2006) the adaptive significance of drought escape in *Avena barbata*, an annual grass. *Evolution* **60**: 2478
- Siddique KHM, Tennant D, Perry MW, Belford RK** (1990) Water use and water use efficiency of old and modern wheat cultivars in a Mediterranean-type environment. *Aus J Agric Res* **41**: 431–447
- Sun XL, Yu QY, Tang LL, Ji W, Bai X, Cai H, Liu XF, Ding XD, Zhu YM** (2013) GsSRK, a G-type lectin S-receptor-like serine/threonine protein kinase, is a positive regulator of plant tolerance to salt stress. *J Plant Physiol* **170**: 505–515
- ten Hove CA, Bochdanovits Z, Jansweijer VMA, Koning FG, Berke L, Sanchez-Perez GF, Scheres B, Heidstra R** (2011) Probing the roles of LRR RLK genes in *Arabidopsis thaliana* roots using a custom T-DNA insertion set. *Plant Mol Biol* **76**: 69–83
- Teotia S, Lamb RS** (2011) RCD1 and SRO1 are necessary to maintain meristematic fate in *Arabidopsis thaliana*. *J Exp Bot* **62**: 1271–1284
- Trapnell C, Pachter L, Salzberg SL** (2009) TopHat: discovering splice junctions with RNA-Seq. *Bioinformatics* **25**: 1105–1111
- Uga Y** (2021) Challenges to design-oriented breeding of root system architecture adapted to climate change. *Breed Sci* **71**: 3–12
- Virlet N, Sabermanesh K, Sadeghi-Tehran P, Hawkesford MJ** (2017) Field Scanalyzer: an automated robotic field phenotyping platform for detailed crop monitoring. *Funct Plant Biol* **44**: 143–153
- Voss-Fels KP, Snowden RJ, Hickey LT** (2018) Designer roots for future crops. *Trends Plant Sci* **23**: 957–960
- Voss-Fels KP, Robinson H, Mudge SR, Richard C, Newman S, Wittkop B, Stahl A, Friedt W, Frisch M, Gabur I, et al.** (2017) *VERNALIZATION1* modulates root system architecture in wheat and barley. *Mol Plant* **11**: 226–229
- Waines JG, Ehdai B** (2007) Domestication and crop physiology: roots of Green-Revolution wheat. *Ann Bot* **100**: 991–998
- Walkowiak S, Gao L, Monat C, Haberer G, Kassa MT, Brinton J, Ramirez-Gonzalez RH, Kolodziej MC, Delorean E, Thambugala D, et al.** (2020) Multiple wheat genomes reveal global variation in modern breeding. *Nature* **588**: 277–283
- Yang Z, Zheng H, Wei X, Song J, Wang B, Sui N** (2018) Transcriptome analysis of sweet Sorghum inbred lines differing in salt tolerance provides novel insights into salt exclusion by roots. *Plant Soil* **430**: 423–439
- Zadoks JC, Chang TT, Konzak CF** (1974) A decimal code for the growth stages of cereals. *Weed Res* **14**: 415–421
- Zelitch I** (1982) The close relationship between net photosynthesis and crop yield. *Bioscience* **32**: 796–802
- Zhu F, Saluja M, Singh JS, Paul P, Sattler SE, Staswick P, Walia H, Yu H** (2021) Phenolmage: an open-source GUI for plant image analysis. *Plant Phenome J* **4**: 20015e